Fuel 344 (2023) 128026

Contents lists available at ScienceDirect

Fuel

journal homepage: www.elsevier.com/locate/fuel

Full Length Article

Bio-hydrogen production from the photocatalytic conversion of wastewater: Parametric analysis and data-driven modelling using nonlinear autoregressive with exogeneous input and back-propagated multilayer perceptron neural networks

Ramesh Kanthasamy [a,*], Imtiaz Ali [a], Bamidele Victor Ayodele [b,c,*], Hisham A. Maddah [a]

[a] Chemical and Materials Engineering Department, Faculty of Engineering Rabigh, King Abdulaziz University, Rabigh 21911, Saudi Arabia
[b] Department of Chemical Engineering, Universiti Teknologi PETRONAS, Seri Iskandar 32610, Perak, Malaysia
[c] Center of Contaminant Control & Utilization (CenCou), Institute of Contaminant Management for Oil and Gas, Universiti Teknologi PETRONAS, Seri Iskandar 32610, Perak, Malaysia

ARTICLE INFO

Keywords:
Biohydrogen
Multilayer perceptron neural networks
Nonlinear autoregressive
Photocatalytic conversion

ABSTRACT

The quest for energy and environmental sustainability necessitates an increasing interest in the photocatalytic conversion of wastewater to biohydrogen. However, the complexity of the photocatalytic conversion and the low productivity of the biohydrogen produced has become a major concern in the scale-up of the process. This study employs a data-driven approach to model biohydrogen production from the photocatalytic conversion of wastewater. Having ascertained the influence of five different parameters namely catalyst size, reaction temperature, catalyst among, irradiation time, and radiation intensity on the biohydrogen production through parametric analysis, the data were employed to model the process using multilayer perceptron neural network (MLPNN) and nonlinear autoregressive neural network (NARX). Both the MLPNN and NARX models were trained using Levenberg-Marquardt (LM), Bayesian regularization (BR), and scaled conjugate gradient (SCG) algorithms. The performance of 20 network architectures was tested for MLPNN-LM, MLPNN-BR, MLPNN-SCG, NARX-LM, NARX-BR, and NARX-SCG. The analysis revealed that the best network architectures of 5-14-1, 5-11-1, 5-7-1, 5-14-1, 5-15-1, and 5-7-1 were obtained for the MLPNN-LM, MLPNN-BR, MLPNN-SCG, NARX-LM, NARX-BR, and NARX-SCG, respectively. All the models demonstrated a good predictability of the biohydrogen production as evidenced by the coefficient of determination (R^2) > 0.9 and low root mean square error (RMSE) values. The best performance was displayed by MLPNN-BR model with R^2 of 0.999 and RMSE of 0.138. The independent variable analysis shows that all the factors significantly influence the predicted biohydrogen production. The catalyst size has the most significant effect on the predicted hydrogen production as indicated by the importance value of 0.329.

1. Introduction

Several industrial processes often result in the generation of a huge amount of wastewater which constitutes an environmental menace [1,2]. The discharge of this untreated wastewater into water bodies is detrimental to human and aquatic lives since they contain a high concentration of toxic organic compounds above the recommended level by environmental protection agencies [3,4]. The wastewater can be sustainably utilized for bioenergy production while simultaneously safeguarding human and aquatic lives [5,6]. Several efforts have been made in developing effective techniques to convert wastewater to bioenergy sources [6–8]. Among the various energy sources, hydrogen has

Abbreviations: ANN, Artificial Neural Network; MLPNN, Multilayer Perceptron Neural Network; NARX, Nonlinear Autoregressive Neural Network; LM, Levenberg-Marquardt; BR, Bayesian Regularization; SCG, Scaled Conjugate Gradient; UV, UltraViolet; GC-TCD-FID, Gas Chromatography-Thermal Conductivity Detector-Flame Ionization; Detector, RMSE; Root Mean Square Error, R^2, Coefficient of Determination.

* Corresponding authors at: Chemical and Materials Engineering Department, Faculty of Engineering Rabigh, King Abdulaziz University, Rabigh 21911, Saudi Arabia (R. Kanthasamy), Department of Chemical Engineering, Universiti Teknologi PETRONAS, Seri Iskandar 32610, Perak, Malaysia (B.V. Ayodele).
E-mail addresses: rsampo@kau.edu.sa (R. Kanthasamy), bamidele.ayodele@utp.edu.my (B.V. Ayodele).

https://doi.org/10.1016/j.fuel.2023.128026
Received 16 January 2023; Received in revised form 17 February 2023; Accepted 28 February 2023
Available online 7 March 2023
0016-2361/© 2023 Elsevier Ltd. All rights reserved.

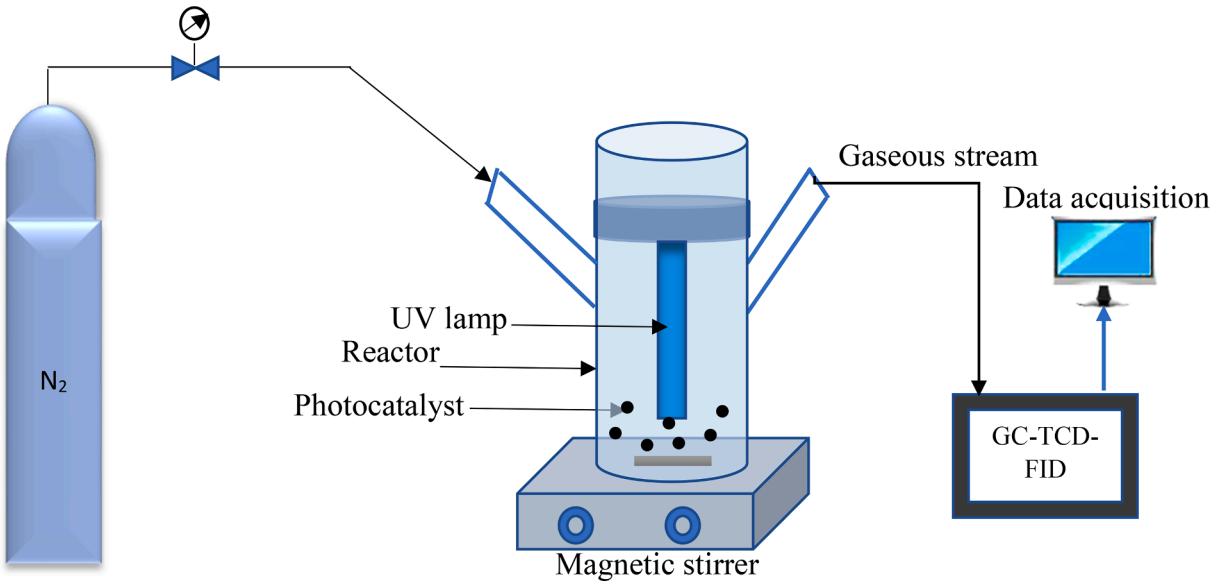

Fig. 1. Typical experimental set-up for photocatalytic reforming of wastewater for hydrogen Production.

been prioritized as the energy of the future due to its numerous advantages [9]. Currently, hydrogen is produced in commercial quantity by a thermo-catalytic pathway that utilizes natural gas as the starting feedstock [10]. Beside the thermo-catalytic pathway, the electrolysis method also significantly contributes to global hydrogen production [11]. Although these well-established pathways for hydrogen production are faced with some challenges such as high energy requirements, environmental concerns from CO_2 emissions, and catalyst deactivation, efforts are being made for improvement through various strategies. As an emerging pathway, it is possible to utilize wastewater from several sources to produce green hydrogen. The green hydrogen produced can in turn be sold as fuels for numerous purposes in various industries.

Hydrogen can be produced from wastewater mainly by biological or photocatalytic techniques which involve the use of microorganisms and photocatalysts, respectively for the conversion of the organic matter in the wastewater to hydrogen [12,13]. An extensive review by Tak et al. [13] revealed that wastewater from the olive mill, juice production, dairy processing, paper, and pulp mill, and oil palm processing industries have been utilized as a source of hydrogen production by photocatalysis and photo-fermentation processes. The effectiveness of the hydrogen production from the various wastewater was tested under different experimental conditions such as catalyst amount, catalyst size, reaction temperature, radiation intensity, and irradiation time. The various studies revealed that the hydrogen yield and production rate differ under different experimental conditions. Hence, to improve the process, it is worthwhile investigating to what extent each of the factors influences the hydrogen yield and production rate. Response surface methodology combined with central composite design and Box-Behnken design has been widely employed to investigate the influence of various factors on hydrogen production using different types of wastewater sources [14–18]. The analyses of the different response surface models revealed that hydrogen production from wastewater was significantly influenced by the stipulated factors. However, the application of response surface methodology and design of experiments often require several experimental runs which is laborious and time-consuming. Besides, it is costly due to the amount of materials required for the process. On the contrary, using a data-driven approach can be less laborious, save time, and be cost-effective.

Data-driven machine learning algorithms such as multilayer perceptron and nonlinear autoregressive neural networks have been widely employed in the modelling of several processes [19–21]. Ayodele et al. [22] employed an MLPNN for modelling catalytic steam methane reforming to hydrogen considering the role of activation functions in the performance of the various models. The study revealed that the MLPNN models had superior performance compared with nonlinear response surface methods. Whiteman et al. [23] compared the performance of MLPNN and response surface methodology in modelling biohydrogen production from sugarcane molasses. The MLPNN models provided a better prediction of the biohydrogen from molasses compared to the response surface models as indicated by R^2 values of 0.91 and 0.75, respectively. Wang et al. [24] employed different data-driven modelling approaches built on MLPNN to model microbial kinetics of biohydrogen production from a dark-fermentation process. The authors revealed that the MLPNN combined a quick convergence, higher accuracy, clear visualization, and direct statistical analysis to accurately model the biohydrogen production from a dark fermentation process. Data-driven algorithms have also been employed for modelling hydrogen production from different wastewater sources. Yogeswari et al. [25] back propagation ANN for modelling hydrogen production from confectionery wastewater. An R^2 of 0.996 obtained from the model performance indicates that the experimental and predicted hydrogen production rate was strongly correlated. Sridevi et al. [26] also employed back propagation ANN for modelling biohydrogen production using distillery wastewater. Using an LM algorithm for training the model, an R^2 of 0.97 was obtained which revealed that the model was robust in modelling the prediction of the biohydrogen from the distillery wastewater. Ghasemian et al. [27] also employed an ANN for the predictive modelling of biohydrogen production from synthetic wastewater. The ANN also shows a robust prediction of the biohydrogen from wastewater. To the best of the authors' knowledge, the application of a hybrid nonlinear autoregressive neural network with exogenous inputs and a back-propagated multilayer perceptron neural network for modelling biohydrogen production from the photocatalytic conversion of wastewater. This study, therefore, explores the robustness of data-driven machine learning techniques such as nonlinear autoregressive neural networks with exogenous inputs and back-propagated multilayer perceptron neural networks for modelling biohydrogen production from the photocatalytic conversion of wastewater.

2. Data acquisition from the photocatalytic conversion of wastewater

Typically, the datasets of the modelling process were acquired from the photocatalytic conversion of wastewater [28,29]. The photocatalytic

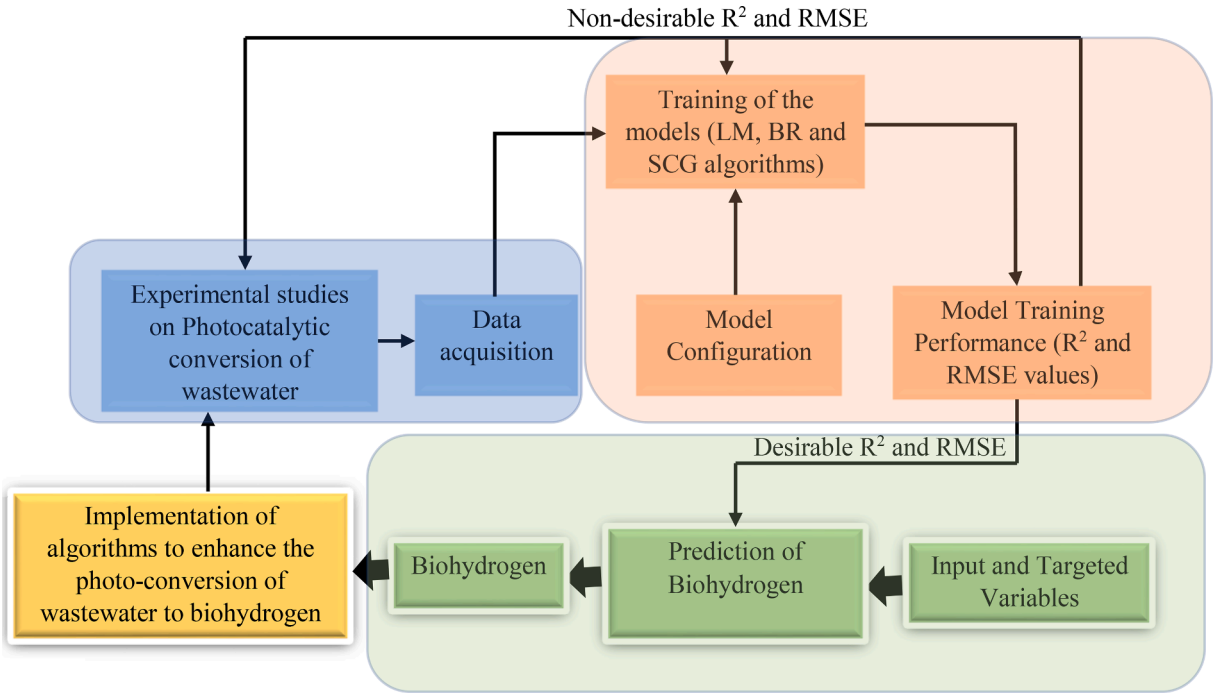

Fig. 2. Schematic representation of the data-driven assisted modelling of biohydrogen from the photocatalytic conversion of wastewater.

system depicted in Fig. 1 consists of a quartz reactor and a light-emitting diode lamp positioned vertically in the reactor which is required for generating the required light intensity by adjusting the distance between the light source and the reactant solution. A specified amount of catalyst was discharged in the wastewater which was placed in the reactor. To prevent the catalyst particles from settling to the bottom of the reactor and losing their active properties, a magnetic stirrer placed underneath the reactor provide continuous stirring. Nitrogen gas served as a carrier gas that was also used to purge the reactor to prevent the accumulation of any dissolved oxygen. The biohydrogen yield was measured from the gaseous stream using gas chromatography with a thermal conductivity detector incorporated with a data-acquisition system.

2.1. Model description, configuration, training, and evaluation

The Backpropagation MLPNN is a feedforward neural network with several layers and is the most popular type of data-driven machine learning algorithm [30]. As a supervised training algorithm, the MLPNN is often regarded as one of the simplest and most general approaches for data-driven modelling. By modifying the weight values, back-propagation MLPNN can approximate the non-linear connection between input and output [22]. In addition, it may be extended to information that was not used in the training process. In back-propagation MLPNN, the feedforward process begins with the application of an input pattern to the network's input layer and continues through the network's layers until the output is generated. For each node contributing to the output, an error signal is calculated by first comparing the actual value produced by the network to the intended value. As all the hidden nodes are responsible, at least in part, for the error observed at the output layer, the signals indicating these errors are sent backward from the output layer to the hidden nodes that made direct contributions to the output layer. This is done layer by layer until each node in the network has received an error signal characterizing its contribution to the overall error. After the error signal has been calculated on every unit, the nodes utilize the errors to adjust the connection weights until the network converges. The backpropagation MLPNN algorithm uses an inbuilt rule with a sigmoid activation function to search for the smallest value of the error function in weight space [31]. In this case, the optimal weights are those that lead to the lowest value for the error function, which solves the learning issue. The processing of the MLPNN can be represented in Eq. (1).

$$\varphi = \vartheta\left(\sum_j w_j x_j + b\right) \tag{1}$$

where ϑ, x_j, w_j and b are the non-linear activation function, the input units, the weights, and the bias.

For sigmoid activation function $\vartheta(x)$ is expressed $\frac{1}{1+e^{-x}}$.

Just like the MLPNN model, the NARX model can be trained to predict time-based data on the series' previous values, which are referred to as feedback delays [32]. The Levenberg-Marquardt, Bayesian regularization, and scale conjugate gradient algorithms were used to train the MLPNN and the NARX models. These models were initially trained in the open-loop version utilizing the actual output rather than feedback. By linking the internal feedback, the open-loop NARX model is converted into a closed-loop version, where real output is substituted by anticipated output to achieve multi-step-ahead prediction.

The performance of any data-driven model is a function of how well-trained the model is. Training a model is the process of extracting optimal values for the model's parameters, such as the weights and the bias, from a dataset [33]. A machine learning method employs empirical risk minimization approach to construct a model in supervised learning by analysing several instances and searching for one that results in the least amount of loss [34]. In this study, three training algorithms namely Levenberg-Marquardt (LM), Bayesian regularization and Scale conjugate descent were used to train the MLPNN and NARX models.

The LM algorithm offers a numerical approach for minimising a nonlinear function [35]. The convergence is both quick and steady. The LM model offers the advantage of combining the he steepest descent method and the Gauss-Newton algorithm [36]. When training with LM algorithm, an increase in the RMSE of the validation samples serves as a signal that training has reached its end and generalisation has stopped getting better. Bayesian regularization (BR) emanated from probabilistic inference of network parameters [37]. This implies that the BM algorithm uses a probability distribution of network weights, as opposed to the deterministic approach of conventional network training, where the

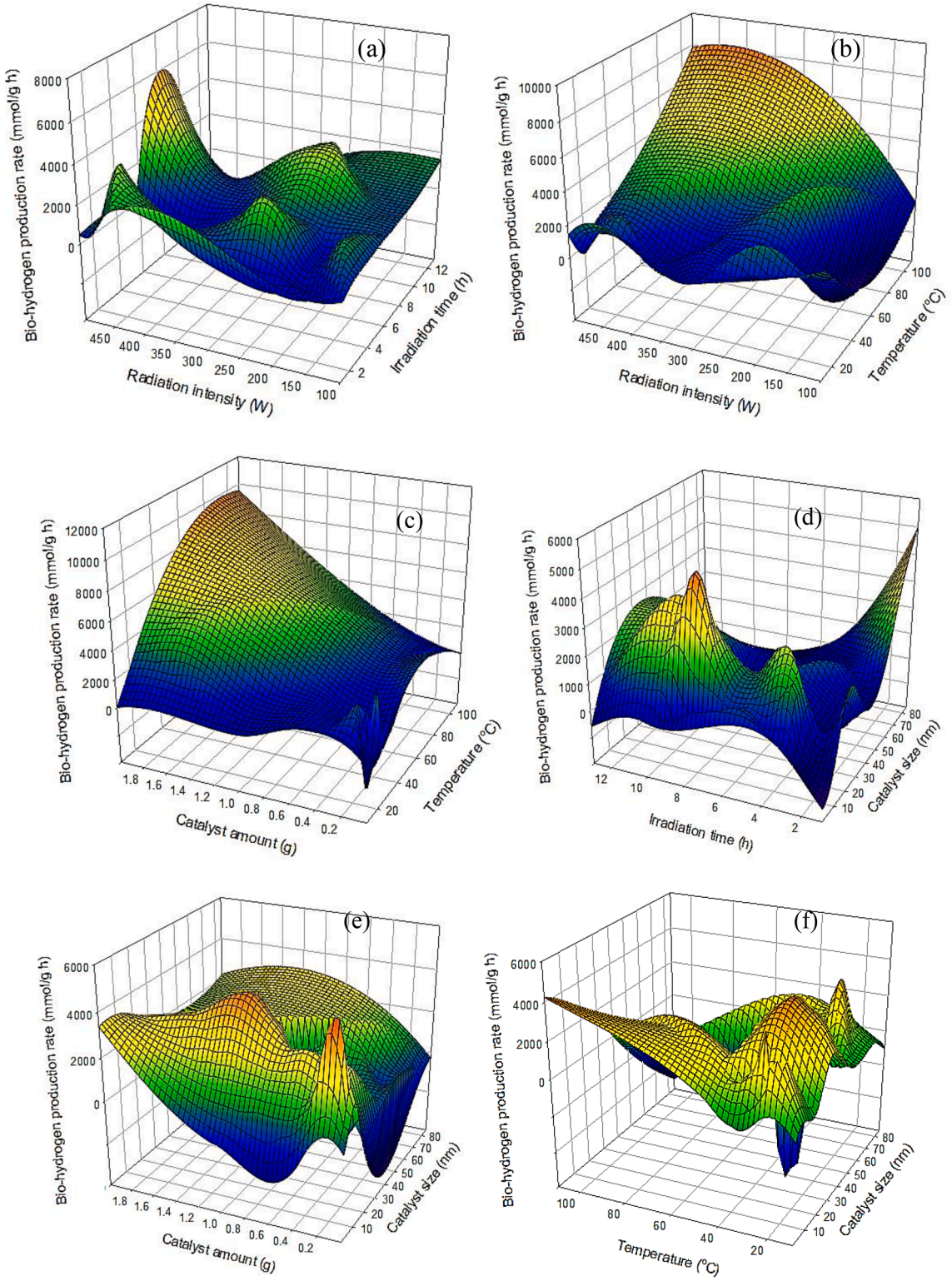

Fig. 3. Interaction effect of (a) Radiation intensity and irradiation time (b) Radiation intensity and temperature (c) Catalyst amount and temperature (d) irradiation time and catalyst size (e) Catalyst amount and catalyst size (f) Temperature and catalyst size on hydrogen production rate.

ideal set of weights is selected by minimizing an error function [38]. Since a probability distribution characterises the network's predictions, it follows that BM has the advantage of great capacity to show potentially complicated linkages. The scaled gradient descent (SCG) algorithm can be employed to search for a local minimum or maximum of a function through an iterative first-order optimization process [39]. Minimizing a cost/loss function using this SCD algorithm is common in data-driving modelling.

The schematic representation of the steps involved in the configuration, training, and evaluation of the MLPNN and NARX models is depicted in Fig. 2. The datasets acquired from the experimental studies on the photocatalytic conversion of wastewater are utilized to train the models. A total of six models namely MLPNN-LM, MLPNN-BR, MLP-SCG, NARX-LM, NARX-BR, and NARX-SCG were evaluated. The best

Table 1
Descriptive statistics of the input and targeted variables.

Factors	Range	Minimum	Maximum	Mean	Standard deviation	Variance	Skewness	Kurtosis
Catalyst size (nm)	84.77	0.23	85.00	14.93	17.80	316.75	2.28	4.84
Reaction temperature (°C)	100.00	10.00	110.00	26.75	12.43	154.47	5.54	37.22
Catalyst amount (g)	1.99	0.01	2.00	0.59	0.41	0.17	0.61	1.00
Irradiation time (h)	12.00	1.00	13.00	5.46	2.55	6.49	0.18	−0.02
Radiation Intensity	400.00	100.00	500.00	228.07	125.59	15772.99	1.23	0.42
Hydrogen production (mmol/h)	4299.00	1.00	4300.00	999.68	956.81	915492.90	1.78	2.95

performance for 20 architectures of each of the models was evaluated based on the coefficient of determination (R^2) (Eq. (2)) and root mean square error (RMSE) (Eq. (3)). For a desirable R^2 and RMSE, the model is deployed to predict biohydrogen production based on input and targeted variables. For non-desirable R^2 and RMSE, the datasets are retrained or re-run from the experimental studies. The datasets were split into 70%, 15%, and 15% for training, testing, and validation. The training, testing, and validation of the model were performed using a machine learning toolbox in MATLAB 2022b (MATHWORK Inc) environment.

$$R^2 = \left(\frac{n(\sum xy) - (\sum x)(\sum y)}{\sqrt{\left[n\sum x^2 - (\sum x)^2\right]\left[n\sum y^2 - (\sum y)^2\right]}} \right)^2 \quad (2)$$

where x is the observed value and y is the predicted value. For a given number of observations (n), the RMSE is given as follows.

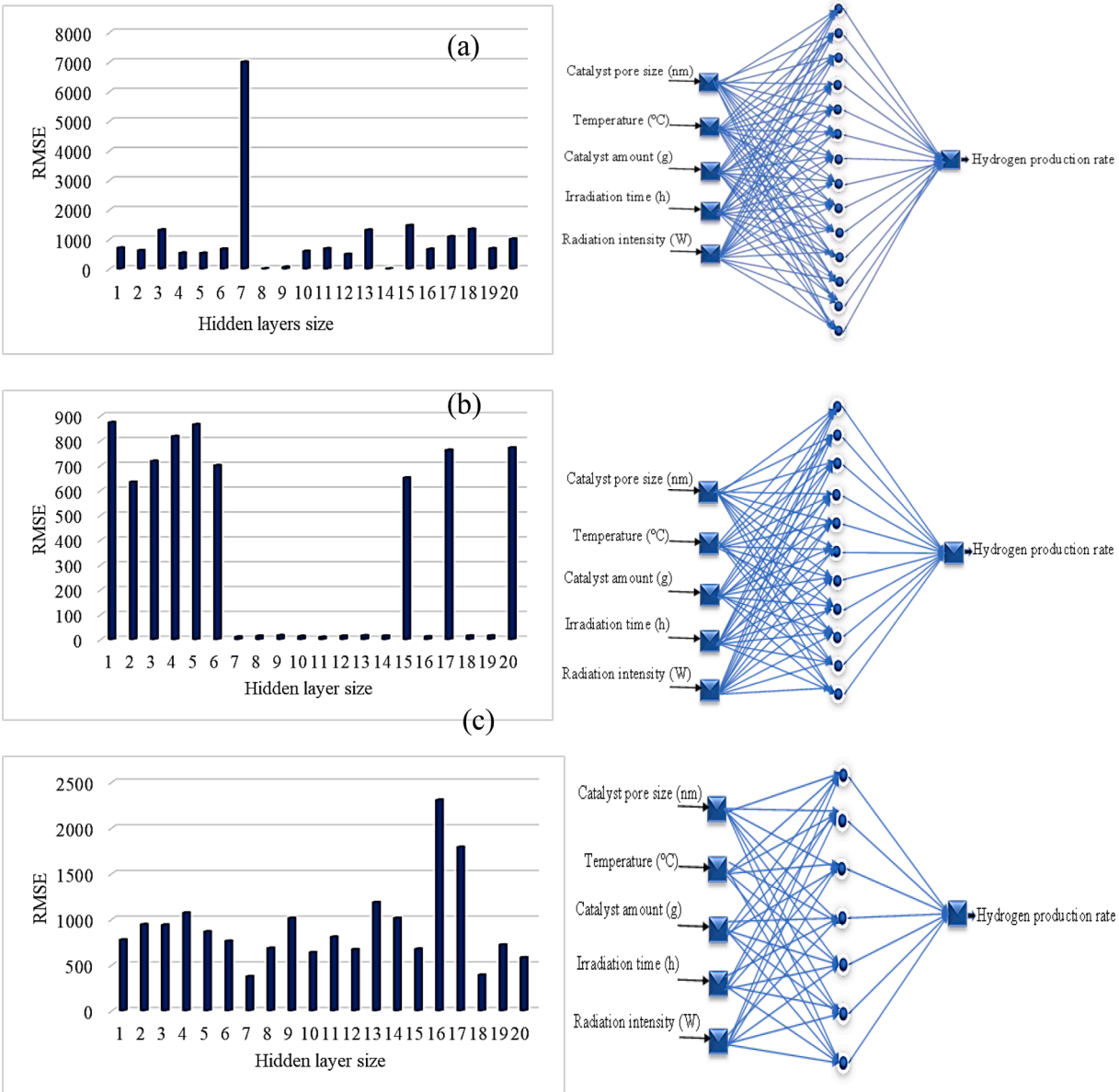

Fig. 4. Network architecture for the (a) MLPNN trained using LM algorithms (b) MLPNN trained using BR algorithms (c) MLP trained using SCG algorithms.

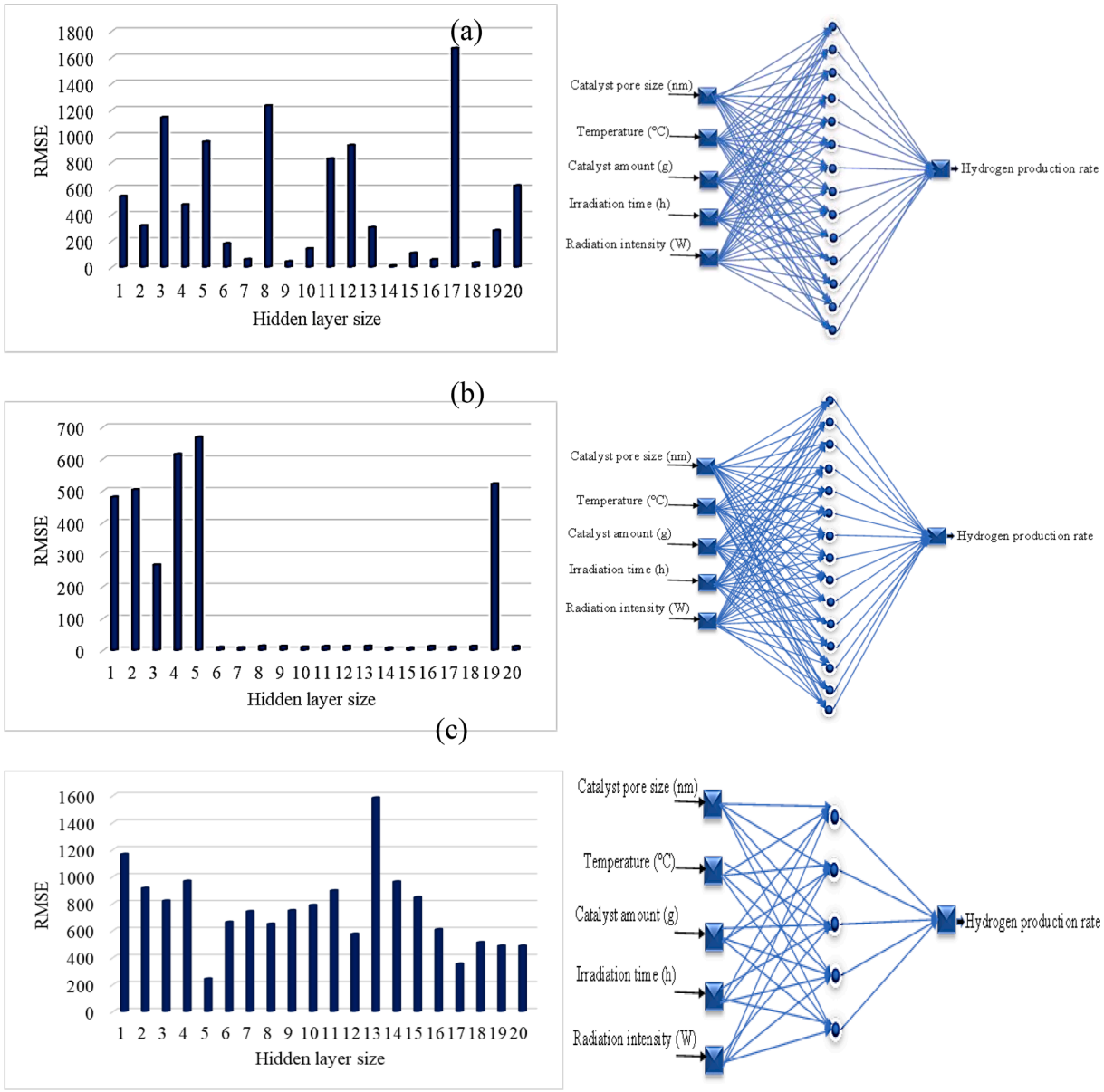

Fig. 5. Network architecture for the (a) NARX trained using LM algorithms (b) NARX trained using BR algorithms (c) NARX trained using SCG algorithms.

$$RMSE = \sqrt{\sum_{i=1}^{n} \frac{(x-y)^2}{n}} \tag{3}$$

The variable importance analysis was performed using modified Garson algorithms represented in Eq. (4) [40,41].

$$\varphi_{ik} = \frac{\sum_{j=1}^{L}\left(\frac{w_{ij}}{\sum_{r=1}^{N} w_{rj}} v_{kj}\right)}{\sum_{i=1}^{N}\left[\sum_{j=1}^{L}\left[\frac{w_{ij}}{\sum_{r=1}^{N} w_{rj}} v_{kj}\right]\right]} \tag{4}$$

3. Results and discussion

3.1. Parametric and descriptive statistical analysis

To evaluate the relationship between the five input parameters and the targeted output, a three-dimensional parametric analysis of the interaction effects was conducted, and the results are presented in Fig. 3 (a)-(f). It can be seen that all the input parameters have a non-linear relationship with the targeted output. Both the radiation intensity and the irradiation time have a non-linear interaction effect with the hydrogen production rate as depicted in Fig. 3 (a). The hydrogen production rate increases with an increase in the radiation intensity and the irradiation time. The most significant influence on the hydrogen production rate can be observed at 10 h irradiation time and 350 W radiation intensity. Similarly, a non-linear relationship also exists between the radiation intensity and the reaction temperature as depicted in Fig. 3 (b). Both the radiation intensity and the reaction temperature have the most significant interaction effect at 450 W and 100 °C, respectively. In Fig. 3 (c), it can be seen that the catalyst amount used for the photoconversion of the wastewater and the temperature of the reaction influence the rate of hydrogen production. Moreover, a non-linear relationship exists between the two parameters. At 100 °C of reaction temperature and 1.8 g of the photocatalysts, a maximum hydrogen rate of 10000 mmol/g/h can be produced. The interaction effect between the irradiation time and nanoparticle size of the catalyst is depicted in Fig. 3 (d). Unlike the trend observed in Fig. 3 (c), there is lesser influence on the rate of hydrogen production between the irradiation time and the nanoparticle size as seen in the lower rate of hydrogen production. The catalyst amount and the nanoparticle size of the catalyst's interaction

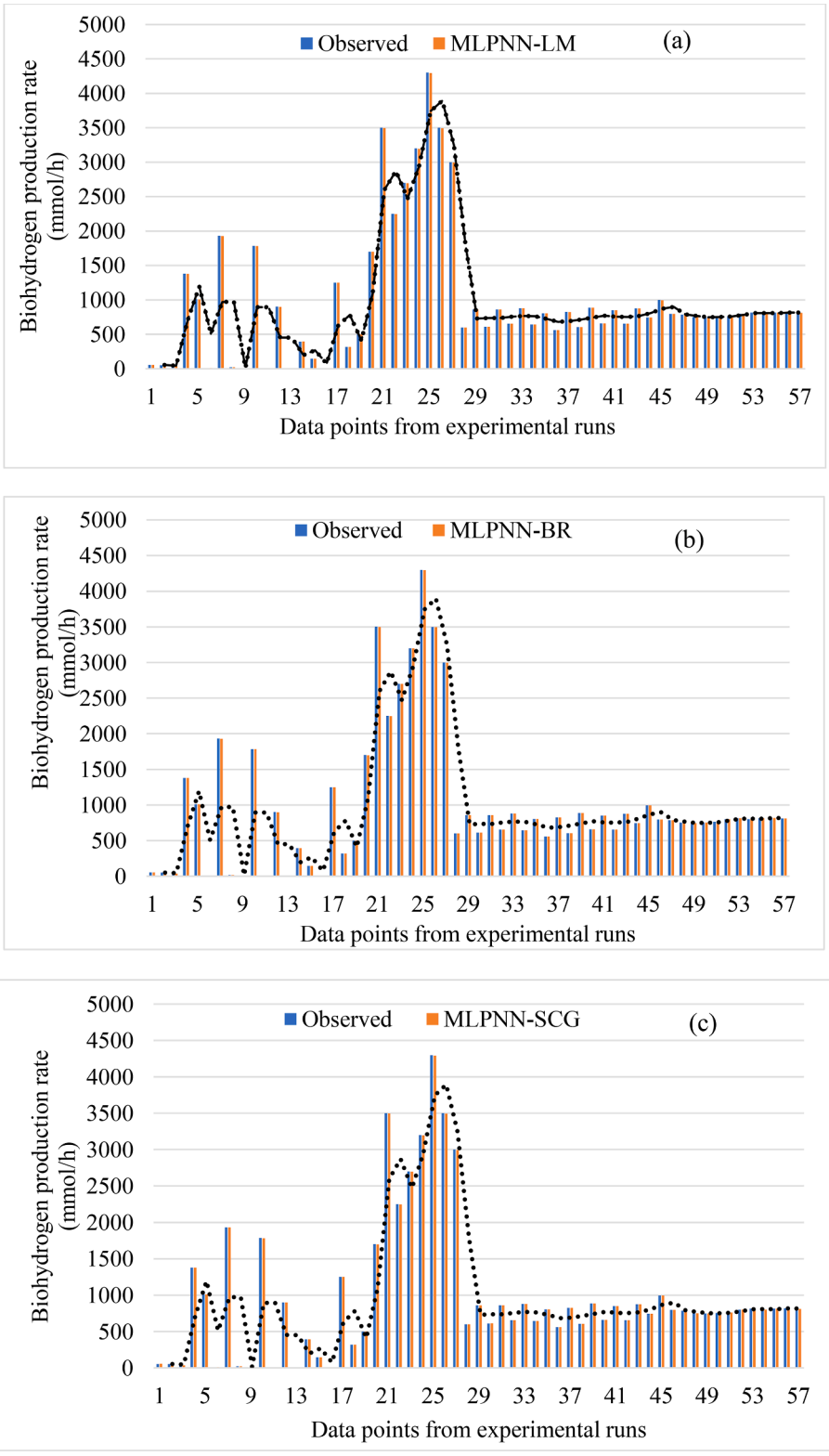

Fig. 6. Comparison between the observed biohydrogen production and (a) MLPNN-LM (b) MLPNN-BR and (c) MLPNN-SCG predicted values.

effect are non-linear and had maximum influence at 50 nm and 100 °C, respectively. Overall, the most significant influence of the interaction effect on the hydrogen production rate from the photocatalytic conversion of wastewater is between the catalyst amount and the reaction temperature. The detailed descriptive statistical analysis of the input and the targeted parameters is summarized in Table 1. In Table 1, the range, minimum values, maximum values, mean, standard deviation, variance, kurtosis, and skewness of the input and targeted parameters are presented for datasets acquired from the experimental runs.

3.2. Evaluation of the best model architecture

Different model architectures were evaluated as a function of the types of training algorithms and the variation in the number of the size

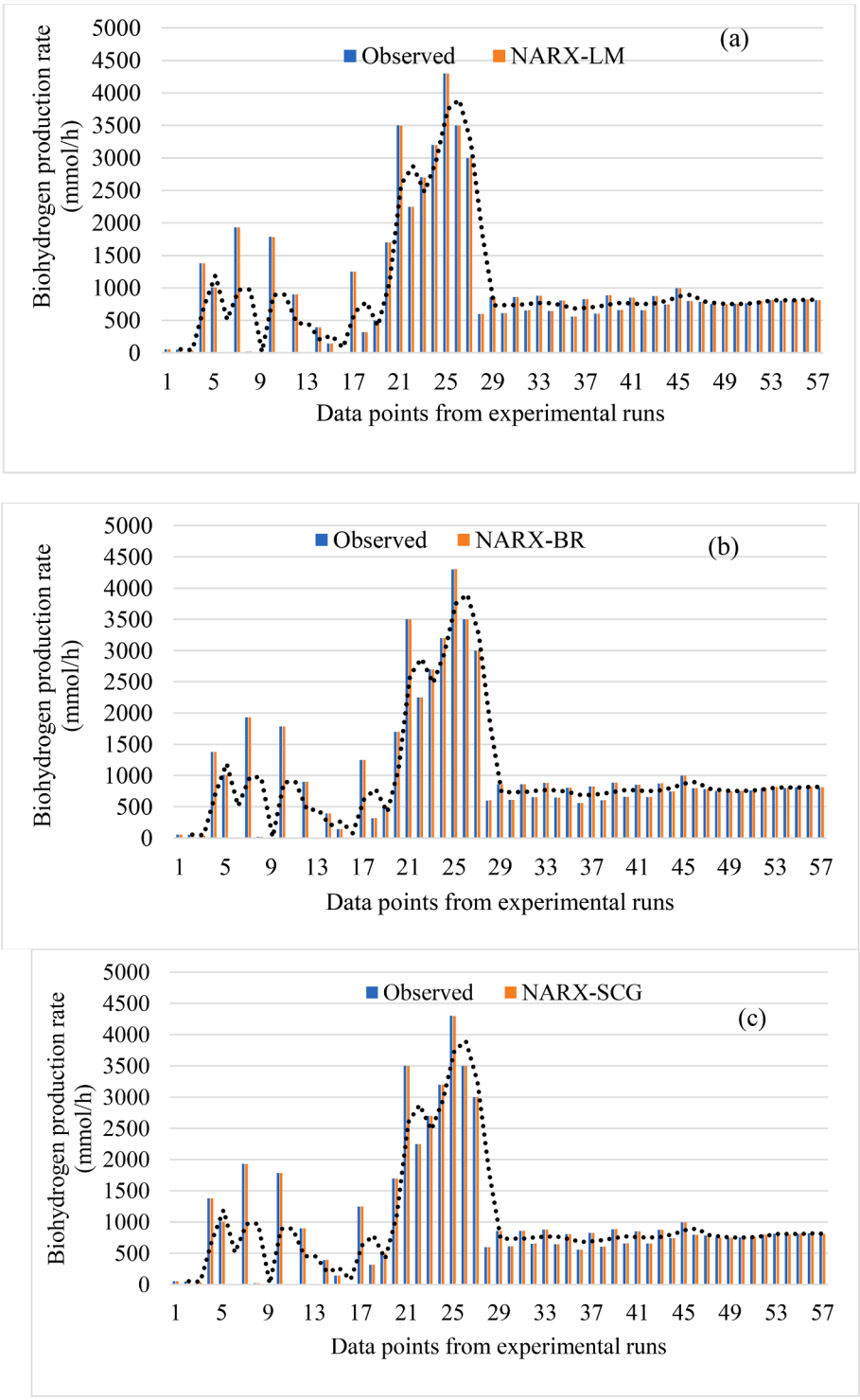

Fig. 7. Comparison between the observed biohydrogen production and (a) NARX-LM (b) NARX-BR and (c) NARX-SCG predicted values.

of the hidden layer. Based on the training algorithms, there are six models namely, MLPNN-LM, MLPNN-BR, MLPNN-SCG, NARX-LM, NARX-BR, and NARX-SCG. The size of the hidden layers was varied from 1 to 20 for each of the models to determine the best performance during training. Figs. 4 and 5 represents the summary of the analysis for each of the model based on the training performance. In Fig. 4 (a), the RMSE obtained for training the MLPNN with the Levenber-Marquardt algorithm varies with the size of the hidden layers. The obtained RMSE values vary from 2.230 to 7000 while the R^2 values are in the range of 0.224 to 0.999. The MLPNN-LM with 5-14-1 architecture has the smallest RMSE values of 2.230 and R^2 of 0.999 and is hence deployed to model the prediction of biohydrogen production. The 5-14-1 architecture of the MLPNN-LM represents five input parameters, 14 hidden neurons, and one targetted input. Fig. 4 (b) shows the performance of the various architectures of the MLPNN-BR as indicated by the RMSE values. The RMSE values vary from 1.023 to 850, while the R^2 values vary from 0.407 to 0.999. The network architecture of 5-11-1 indicating 5 input parameters, 11 artificial neurons in the hidden layer and 1 targeted output has the least RMSE of 1.023 and R^2 of 0.999 hence deployed for modeling the biohydrogen prediction from the

Table 2
Best network architecture from each of the models.

Models	Architecture	R^2	MSE	RMSE
MLPNN-LM	5-14-1	0.997	4.597	2.144
MLPNN-BR	**5-11-1**	**0.999**	**0.019**	**0.138**
MLPNN-SCG	5-7-1	0.998	3.846	1.961
NARX-LM	5-14-1	0.999	1.304	1.142
NARX-BR	**5-15-1**	**0.999**	**0.076**	**0.276**
NARX-SCG	5-5-1	0.998	1.445	1.202

photocatalytic conversion of the wastewater. In Fig. 4 (c), the RMSE values for the MLPNN-SCG vary from 300 to 2300 while the R^2 varies from 0.261 to 0.999. The network architecture of 5-7-1 which indicates 5 input units, 7 artificial neurons in the hidden layers and 1 targeted output has the least RMSE of 300 and R^2 of 0.999. Hence, also employed to predict the biohydrogen production from the photocatalytic conversion of the wastewater.

Similar to the MLPNN-based network architecture performance evaluation, different network architectures were also evaluated for the NARX-LM, NARX-BR, and NARX-SCG. The performance of each of the architectures as a function of the RMSE values is summarized in Fig. 5. As shown in Fig. 5 (a), the RMSE values for each of the network architectures vary from 1.432 to 1620. The NARX network with an architecture of 5-14-1 indicating 5 input units, 14 artificial neurons at the hidden layer and 1 output unit have the least RMSE values of 1.432 and R^2 of 0.999. The 5-14-1 NARX-LM model was subsequently deployed to predict the biohydrogen production from the photocatalytic conversion of wastewater. In Fig. 5 (b), the performance of the NARX-BR model as a function of the RMSE values of the various architectures is presented. The RMSE of each of the NARX-BR network architectures varies with the changes in the size of the hidden layers. The RMSE of the various architecture ranges from 1.534 to 650 and R^2 ranges from 0.407 to 0.999. The NARX-BR architecture of 5-15-1 indicating 5 input units, 15 artificial neurons in the hidden layers and 1 output unit has the least RMSE values of 1.534 and R^2 of 0.999. Hence, the 5-15-1 NARX-BR model was subsequently deployed for the prediction of the Biohydrogen from the photocatalytic conversion of wastewater. Fig. 5 (c) displays the various RMSE values of each of the NARX-SCG architectures and the final architecture. The RMSE values of each of the NARX-SCG architectures vary with changes in the size of the artificial neurons in the hidden layer. The NARX-SCG with 5-5-1 architecture indicating 5 input units, 5 artificial neurons in the hidden layer and 1 output unit have the least RMSE of 1.524 and R^2 of 0.999. Hence, the 5-5-1 NARX-SCG architecture was employed to predict the biohydrogen production from the photocatalytic conversion of the wastewater.

3.3. Performance analysis of MLPNN models in the prediction of the biohydrogen

The performance analysis of the MLPNN and NARX architectures in modelling the prediction of biohydrogen from the photocatalytic conversion of wastewater are depicted in Figs. 6 and 7. While the performance matrices in terms of the network architecture, R^2, MSE, and RMSE are summarized in Table 2. All three MLPNN-based models displayed good predictability as depicted in Fig. 6(a)-(c). In Fig. 6 (a), the predicted biohydrogen production rate for each of the experimental points is consistent with the observed values obtained from the experimental runs. The consistency of the predicted and the observed values of the biohydrogen production rates can be confirmed by the R^2 values of 0.997 and RMSE of 2.144. The robustness of the MLPNN-LM in modelling the determination of the optimal structure for the prediction of dynamic viscosity of oil-based hybrid nanofluid has been reported by Hemmat Esfe et al. [42]. The rheology characteristics of the oil-based hybrid nanofluid were accurately predicted by the optimized MLPNN-LM with 8 neurons as indicated by R^2 of 0.999 and MSE of 4.73×10^{-5}. Also, Ouadfeul et al. [43] reported the efficiency of MLPNN-LM in predicting total organic carbon in shale gas reservoirs. The performance of the MLPNN-BR in predicting the biohydrogen production rate from the photocatalytic conversion of wastewater is depicted in Fig. 6 (b). Similar to the MLPNN-LM, the MLPNN-BR performed well in predicting the biohydrogen production from the photocatalytic conversion of the wastewater. As shown in Table 2, the predicted biohydrogen production rates obtained from the 5-11-1 MLPNN-BR network are consistent with the experimental values. This can be confirmed by the R^2 of 0.999, which implies that the predicted and the observed values are strongly correlated with minimal prediction error (RMSE of 0.138). Haiqi et al. [44] had reported the robustness of the MLPNN-BR in predicting the modelling of photocatalytic phenol degradation from oil field-produced wastewater. As indicated by R^2 of 0.999, the predicted photocatalytic phenol degradation is strongly correlated with the experimental values with a predicted error of 1.27. Also, MLPNN-BR was robust in modelling the prediction of the mass attenuation coefficient of gamma radiation as reported by Moshkbar-Bakhshayesh et al. [45]. This is evident from the R^2 of 0.990, an indication that the predicted mass attenuation coefficient of gamma radiation is consistent with the experimental values. The performance of the MLPNN-SCG in modelling the prediction of the biohydrogen production rate from the photocatalytic conversion of wastewater is depicted in Fig. 6 (c). The predicted biohydrogen production rates are strongly correlated with the observed values obtained from the experimental runs. The 5-7-1 MLPNN-SCG network also displayed a strong capability in modelling the prediction of the biohydrogen as indicated by R^2 of 0.998 and RMSE values of 1.961. Yusoff et al. [46] employed MLPNN-SCG network to examine the effect of nanosilica modified bitumen in unaged and aged conditions. The study revealed that there is a strong correlation between the measured and predicted data depicting the ability of the MLPNN-SCG to efficiently model the inter-relationship between the input and the output parameters.

3.4. Performance analysis of NARX models in the prediction of the biohydrogen

The performance of the NARX models trained using the LM, BR, and SCG algorithms are depicted in Fig. 6. The optimized network architecture of 5-14-1, 5-15-1, and 5-5-1 were employed to model the biohydrogen prediction using the NARX-LM, NARX, and NARX-SCG, respectively. As shown in Fig. 6 (a), the predicted biohydrogen production rate by the NARX-LM models is consistent with the observed values obtained from each point of the experimental runs. As evidenced by the R^2 of 0.999, an indication of a strong correlation between the predicted biohydrogen production and the observed values with an RMSE of 1.142. Mohd et al. [47] reported the robustness of the NARX-LM used for modelling rainfall prediction. Also, Guzman et al. [48] successfully employed NARX-LM for modelling the prediction of daily groundwater levels. The performance of the NARX-BR in modelling biohydrogen prediction from wastewater is depicted in Fig. 6 (b). The observed biohydrogen production rate obtained from the experimental runs is consistent with the predicted values obtained from the NARX-BR model. With R^2 of 0.999 and RMSE of 0.276, the optimized 5-15-1 NARX-BR model robustly models the non-linear relationship between the various input parameters and the targeted output. The robustness of the NARX-BR in modelling the prediction of vertical track irregularities from the high-speed line has been reported by Jiang et al. [49]. Similarly, Al Jami et al. [50] reported the superior capability of the NARX-BR for the prediction of groundwater level. The predictability of the optimized 5-5-1 NARX-SCG model is depicted in Fig. 6 (c). At each of the data points, the predicted biohydrogen production rate by the NARX-SCG model and the observed values are in proximity. The R^2 of 0.998 obtained for the prediction of the biohydrogen production rate by the NARX-SCG model indicate the that the predicted values are strongly correlated with prediction errors of 1.202. The robustness of the NARX-

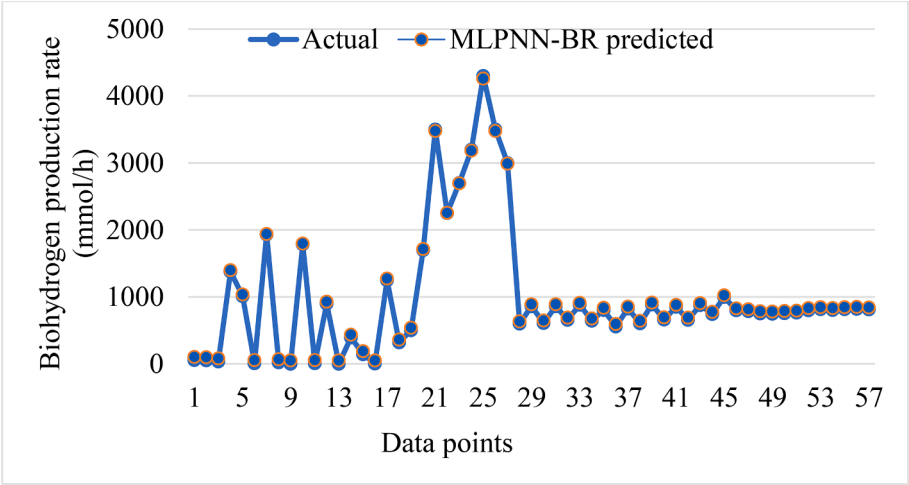

Fig. 8. Comparison between the actual biohydrogen production rate and the predicted values by the best model (MLPNN-BR).

SCG in predicting the biohydrogen production rate is consistent with that reported by Nekoee et al. [51] for modelling the prediction of earthquake occurrence time. The predictive capability of the NARX-SCG in modelling the prediction of hourly solar radiation has been reported by Mohammed et al. [52].

3.5. Model performance validation

The performance of the models was validated using the R^2, MSE, and RMSE as summarized in Table 2. The R^2, which ranges from 0 to 1, expresses how accurate the prediction of a model. The R^2 may be seen as the percentage of variance in the dependent variable that the statistical model predicts. The R^2 helps to analyze the degree to which variations in one variable can be accounted for by variations in another. When evaluating a model's performance, whether during training or validation, it is incredibly beneficial to determine the prediction error which is a function of the MSE and RMSE. The RMSE is a commonly used metric for determining how accurate a model is in predicting quantitative data [49,53,54]. As shown in Table 2, all the six models performed well in predicting the biohydrogen production rate from the wastewater as indicated by the R^2 values. The $R^2 > 0.9$ is an indication that the actual biohydrogen production rates obtained from the bioconversion of the wastewater are strongly correlated with the predicted values from the models. However, further analysis using the MSE and the RMSE shows that the prediction errors of each model vary. The MLPNN-LM has the highest MSE and RMSE of 4.597 and 2.144, respectively. While the MLPNN-BR has the lowest MSE and RMSE of 0.019 and 0.138, respectively. This implied that he MLPNN-BR model is more robust in modelling the biohydrogen production rate from the bioconversion of the wastewater with minimized errors compared to the other models. As shown in Fig. 8, both the actual and the predicted biohydrogen production rates are strongly correlated. It can be seen that the BR algorithm plays a significant role in the model performance [37,55]. The BR algorithm has the capability to detect and learn a complex relationship between the model input and the targets [56].

3.6. Comparison of the best model with literature and study implication

Although the six MLPNN and NARX-based data-driven models evaluated for prediction of biohydrogen production from the photocatalytic conversion of wastewater displayed good capability as indicated by the high R^2. However, the MLPNN-BR and NARX-BR models have the most robust capability as indicated by the high R^2 and low RMSE values. It is obvious that the use of the Bayesian regularization algorithm to train the MLPNN and NARX models significantly enhances the performance compared with the Levenberg-Marquardt and Scaled Conjugate gradient algorithms. The requirement for extensive cross-validation can be decreased or eliminated with Bayesian regularised MLPNN and NARX which are more resilient than traditional back-propagation algorithms. With the incorporation of the Bayesian regularization algorithms, the MLPNN and NARX are resilient in modelling the non-linear relationship between the input and targeted parameters. Thereby resulting in a robust prediction of biohydrogen with minimized errors as indicated by the RMSE values. The performance of the MLPNN-BR and NARX-BR model obtained from this study is comparable with that reported in the literature (Table 3) for modelling explosion risk analysis of the fixed offshore platforms, parameter extraction from proton exchange membrane fuel cell, Strength Characteristics of Fly-Ash and Bottom-Ash prediction, load prediction in district building and hydraulic Fracturing Fluid Leakage as indicated by the R^2 and RMSE values. The variation in the prediction capacity of each of the models in Table 3 can be due to the differences in the features, nature of datasets, and the network architectures. The independent variable importance was conducted for the MLPNN-BR since it outperformed the other models. As shown in Fig. 8, all the input variables have varying levels of influence on the predicted biohydrogen production rate. The predicted biohydrogen production rate can be seen to be most influenced by the catalyst size and least influenced by the irradiation time. This analysis can help with the decision of incorporating necessary measures to

Table 3
Comparison of the study with the literature.

Model-type	Function	R^2	RMSE	Reference
MLPNN-BR	Modelling of biohydrogen production rate from photo-conversion of wastewater	0.999	0.138	This study
NARX-BR	Modelling of biohydrogen production rate from photo-conversion of wastewater	0.999	0.276	This study
MLPNN-BR	Modelling of explosion risk analysis of fixed offshore platform	0.988	N.R.	[37]
MLPNN-BR	Modelling parameter extraction from proton exchange membrane fuel cell	N. R	0.086*	[57]
MLPNN-BR	Modelling Strength Characteristics of Fly-Ash and Bottom-Ash prediction	0.981	1.378	[58]
MLPNN-BR	Modelling of load prediction in the district building	N.R.	91.01	[59]
NARX-BR	Modelling of hydraulic Fracturing Fluid Leakage	0.944	0.0049	[60]

* Converted to fraction, N.R is not reported.

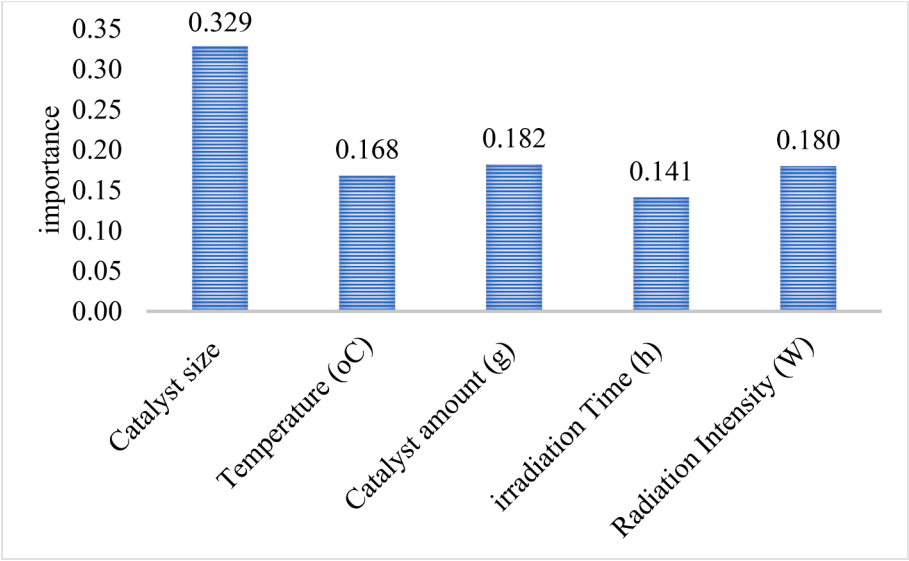

Fig. 9. Input variable importance analysis in the MLPNN-BR model output.

optimize the parameters that significantly influence the biohydrogen production rate in the eventuality of a scale-up process (Fig. 9).

4. Conclusion

The parametric analysis and application of MLPNN and NARX models trained with Levenberg-Marquardt, Bayesian Regularization, and Scaled Conjugate Gradient algorithms for the prediction of biohydrogen production from the photocatalytic conversion of wastewater have been reported in this study. The changes in the numbers of artificial neurons in the hidden layers of 20 network architectures of each of the models significantly influence the model outputs. Optimized The analysis revealed that the best network architectures of 5-14-1, 5-11-1, 5-7-1, 5-14-1, 5-15-1, and 5-7-1 were obtained for the MLPNN-LM, MLPNN-BR, MLPNN-SCG, NARX-LM, NARX-BR, and NARX-SCG. The optimized MLPNN-LM, MLPNN-BR, MLPNN-SCG, NARX-LM, NARX-BR, and NARX-SCG models displayed robust capabilities in modelling the biohydrogen production from the photocatalytic conversion of wastewater. The predictabilities of the models resulted in high R^2 values (>0.9) indication the ability of the inbuilt algorithms to learn the non-linear relationship between the input variable and the targeted output. The MLPNN-BR having the least RMSE of 0.138 displayed the best predictive performance. The independent variable importance analysis of the MLPNN-BR model revealed that the catalyst size, reaction temperature, catalyst amount, irradiation time, and radiation intensity have a significant influence on the predicted biohydrogen production rate. The catalyst size with an importance value of 0.329 has the most significant influence on the predicted biohydrogen production rate by the MLPNN-BR model.

CRediT authorship contribution statement

Ramesh Kanthasamy: Conceptualization, Funding acquisition, Writing – review & editing. **Imtiaz Ali:** Visualization, Validation, Writing – review & editing. **Bamidele Victor Ayodele:** Conceptualization, Methodology, Writing – review & editing. **Hisham Maddah:** Writing – review & editing.

Declaration of Competing Interest

The authors declare that they have no known competing financial interests or personal relationships that could have appeared to influence the work reported in this paper.

Data availability

Data will be made available on request.

Acknowledgements

This research work was funded by Institutional Fund Projects under grant no (IFPIP: 1523-829-1442). Therefore, authors gratefully acknowledge technical and financial support from the Ministry of Education and King Abdulaziz University, DSR, Jeddah, Saudi Arabia.

References

[1] Jiménez S, Micó MM, Arnaldos M, Medina F, Contreras S. State of the art of produced water treatment. Chemosphere 2018;192:186–208. https://doi.org/10.1016/j.chemosphere.2017.10.139.
[2] Varjani S, Joshi R, Srivastava VK, Ngo HH, Guo W. Treatment of wastewater from petroleum industry: current practices and perspectives. Environ Sci Pollut Res 2020;27:27172–80. https://doi.org/10.1007/s11356-019-04725-x.
[3] Inyang IR, Izah SC, Suobo K. Effect of Phenol on the Kidney and Liver Biochemical and Metabolites of Clarias Gariepinus. Noble Int J Sci Res 2019;03:33–40.
[4] Mg R, Girigoswami A. Bisphenol A-an Overview on its Effect on Health and Environment. Biointerface Res Appl Chem 2021;12:105–19. https://doi.org/10.33263/briac121.105119.
[5] Abubackar HN, Keskin T, Yazgin O, Gunay B, Arslan K, Azbar N. Biohydrogen production from autoclaved fruit and vegetable wastes by dry fermentation under thermophilic condition. Int J Hydrogen Energy 2019. https://doi.org/10.1016/j.ijhydene.2018.12.068.
[6] Meier TRW, Cremonez PA, Maniglia TC, Sampaio SC, Teleken JG, da Silva EA. Production of biohydrogen by an anaerobic digestion process using the residual glycerol from biodiesel production as additive to cassava wastewater. J Clean Prod 2020;:258. https://doi.org/10.1016/j.jclepro.2020.120833.
[7] Bhatia SK, Mehariya S, Bhatia RK, Kumar M, Pugazhendhi A, Awasthi MK, et al. Wastewater based microalgal biorefinery for bioenergy production: Progress and challenges. Sci Total Environ 2021;751:141599.
[8] Goswami RK, Mehariya S, Verma P, Lavecchia R, Zuorro A. Microalgae-based biorefineries for sustainable resource recovery from wastewater. J Water Process Eng 2021;40:101747. https://doi.org/10.1016/j.jwpe.2020.101747.
[9] Ayodele BV, Mustapa SI, Tuan Abdullah TAR, Bin SSF. A Mini-Review on Hydrogen-Rich Syngas Production by Thermo-Catalytic and Bioconversion of Biomass and Its Environmental Implications. Front Energy Res 2019;7:1–6. https://doi.org/10.3389/fenrg.2019.00118.
[10] Hosseini SE, Wahid MA. Hydrogen production from renewable and sustainable energy resources: Promising green energy carrier for clean development. Renew Sustain Energy Rev 2016;57:850–66. https://doi.org/10.1016/j.rser.2015.12.112.
[11] Dincer I, Acar C. Review and evaluation of hydrogen production methods for better sustainability. Int J Hydrogen Energy 2015;40:11094–111. https://doi.org/10.1016/j.ijhydene.2014.12.035.
[12] Ayodele BV, Abdullah TARBT, Alsaffar MA, Mustapa SI, Salleh SF. Recent advances in renewable hydrogen production by thermo-catalytic conversion of biomass-derived glycerol: Overview of prospects and challenges. Int J Hydrogen Energy 2020;45:18160–85. https://doi.org/10.1016/j.ijhydene.2019.08.002.

[13] Tak SS, Shetye O, Muley O, Jaiswal H, Malik SN. Emerging technologies for hydrogen production from wastewater. Int J Hydrogen Energy 2022;47:37282–301. https://doi.org/10.1016/j.ijhydene.2022.06.225.
[14] Nasution A, Ali E, Yaakob Z. Electrocoagulation of palm oil mill effluent for treatment and hydrogen production using response surface methodology. Polish J Environ Stud 2014;23:1669–77.
[15] Wang J, Wan W. Optimization of fermentative hydrogen production process by response surface methodology. Int J Hydrogen Energy 2008;33:6976–84. https://doi.org/10.1016/j.ijhydene.2008.08.051.
[16] Yin Y, Wang J. Optimization of Hydrogen Production by Response Surface Methodology Using γ-Irradiated Sludge as Inoculum. Energy Fuel 2016;30:4096–103. https://doi.org/10.1021/acs.energyfuels.6b00262.
[17] Gadhe A, Sonawane SS, Varma MN. Optimization of conditions for hydrogen production from complex dairy wastewater by anaerobic sludge using desirability function approach. Int J Hydrogen Energy 2013;38:6607–17. https://doi.org/10.1016/j.ijhydene.2013.03.078.
[18] Hitit ZY, Lazaro CZ, Hallenbeck PC. Hydrogen production by co-cultures of Clostridium butyricum and Rhodospeudomonas palustris: Optimization of yield using response surface methodology. Int J Hydrogen Energy 2017;42:6578–89. https://doi.org/10.1016/j.ijhydene.2016.12.122.
[19] Ahmad J, Awais M, Rashid U, Ngamcharussrivichai C, Raza Naqvi S, Ali I. A systematic and critical review on effective utilization of artificial intelligence for bio-diesel production techniques. Fuel 2023;338:127379. https://doi.org/10.1016/j.fuel.2022.127379.
[20] Aslam Khan MN, Haq ZU, Ullah H, Naqvi SR, Ahmed U, Zaman M, et al. Prediction of hydrogen yield from supercritical gasification process of sewage sludge using machine learning and particle swarm hybrid strategy. Int J Hydrogen Energy 2023. https://doi.org/10.1016/j.ijhydene.2023.01.033.
[21] khan M, Raza Naqvi S, Ullah Z, Ali Ammar Taqvi S, Nouman Aslam Khan M, Farooq W, et al. Applications of machine learning in thermochemical conversion of biomass-A review. Fuel 2023;332:126055.
[22] Ayodele BV, Alsaffar MA, Mustapa SI, Adesina A, Kanthasamy R, Witoon T, et al. Process intensification of hydrogen production by catalytic steam methane reforming: Performance analysis of multilayer perceptron-artificial neural networks and nonlinear response surface techniques. Process Saf Environ Prot 2021;156:315–29.
[23] Whiteman JK, Gueguim Kana EB. Comparative Assessment of the Artificial Neural Network and Response Surface Modelling Efficiencies for Biohydrogen Production on Sugar Cane Molasses. BioEnergy Res 2014;7:295–305. https://doi.org/10.1007/s12155-013-9375-7.
[24] Wang Y, Tang M, Ling J, Wang Y, Liu Y, Jin H, et al. Modeling biohydrogen production using different data driven approaches. Int J Hydrogen Energy 2021;46(58):29822–33.
[25] Yogeswari MK, Dharmalingam K, Mullai P. Implementation of artificial neural network model for continuous hydrogen production using confectionery wastewater. J Environ Manage 2019;252:109684. https://doi.org/10.1016/j.jenvman.2019.109684.
[26] Sridevi K, Sivaraman E, Mullai P. Back propagation neural network modelling of biodegradation and fermentative biohydrogen production using distillery wastewater in a hybrid upflow anaerobic sludge blanket reactor. Bioresour Technol 2014;165:233–40. https://doi.org/10.1016/j.biortech.2014.03.074.
[27] Ghasemian M, Taheri E, Fatehizadeh A, Amin MM. Biological hydrogen production from synthetic wastewater by an anaerobic migrating blanket reactor: Artificial neural network (ANN) modeling. Environ Heal Eng Manag J 2019;6(4):269–76.
[28] Munusamy TD, Chin SY, Khan MMR. Optimization of process parameters for photoreforming of hydrogen evolution via response surface methodology (RSM): A study using Carbon@exfoliated g–C3N4. Chem Eng Res Des 2022;177:513–25. https://doi.org/10.1016/j.cherd.2021.10.028.
[29] Bosu S, Rajamohan N. Influence of nanomaterials in biohydrogen production through photo fermentation and photolysis - Review on applications and mechanism. Int J Hydrogen Energy 2022. https://doi.org/10.1016/j.ijhydene.2022.09.062.
[30] Zeng Y-R, Zeng Y, Choi B, Wang L. Multifactor-influenced energy consumption forecasting using enhanced back-propagation neural network. Energy 2017;127:381–96. https://doi.org/10.1016/j.energy.2017.03.094.
[31] Lenzi GG, Evangelista RF, Duarte ER, Colpini LMS, Fornari AC, Menechini Neto R, et al. Photocatalytic degradation of textile reactive dye using artificial neural network modeling approach. Desalin Water Treat 2016;57(30):14132–44.
[32] Mustapa SI, Ayodele FO, Ayodele BV, Mohammad N. Nexus between energy usability, economic indicators and environmental sustainability in four asean countries: A non-linear autoregressive exogenous neural network modelling approach. Processes 2020;8:1–20. https://doi.org/10.3390/pr8121529.
[33] Jazayeri K, Jazayeri M, Uysal S. Comparative analysis of levenberg-marquardt and bayesian regularization backpropagation algorithms in photovoltaic power estimation using artificial neural network. Lect Notes Comput Sci (Including Subser Lect Notes Artif Intell Lect Notes Bioinformatics) 2016;9728:80–95. https://doi.org/10.1007/978-3-319-41561-1_7.
[34] Huang L, Zhang C, Zhang H. Self-adaptive training: Beyond empirical risk minimization. Adv Neural Inf Process Syst 2020;2020-December:1–12.
[35] Garoosiha H, Ahmadi J, Bayat H, Formisano A. The assessment of Levenberg–Marquardt and Bayesian Framework training algorithm for prediction of concrete shrinkage by the artificial neural network. Cogent Eng 2019;6(1).
[36] Ye Z, Kim MK. Predicting electricity consumption in a building using an optimized back-propagation and Levenberg–Marquardt back-propagation neural network: Case study of a shopping mall in China. Sustain Cities Soc 2018;42:176–83. https://doi.org/10.1016/j.scs.2018.05.050.
[37] Shi J, Zhu Y, Khan F, Chen G. Application of Bayesian Regularization Artificial Neural Network in explosion risk analysis of fixed offshore platform. J Loss Prev Process Ind 2019;57:131–41. https://doi.org/10.1016/j.jlp.2018.10.009.
[38] Douak M, Settou N. Estimation of Hydrogen Production Using Wind Energy in Algeria. Energy Proc 2015;74:981–90. https://doi.org/10.1016/j.egypro.2015.07.829.
[39] Mageed AK. Modeling photocatalytic hydrogen production from ethanol over copper oxide nanoparticles: a comparative analysis of various machine learning techniques. Biomass Convers Biorefinery 2023;13(4):3319–27.
[40] Garson GD. Comparison of Neural Network Analysis of Social Science Data. Soc Sci Comput Rev 1991;9:399–434.
[41] Goh ATC. Back-propagation neural networks for modeling complex systems. Artif Intell Eng 1995;9:143–51. https://doi.org/10.1016/0954-1810(94)00011-S.
[42] Hemmat Esfe M, Amoozadkhalili F, Toghraie D. Determining the optimal structure for accurate estimation of the dynamic viscosity of oil-based hybrid nanofluid containing MgO and MWCNTs nanoparticles using multilayer perceptron neural networks with Levenberg-Marquardt Algorithm. Powder Technol 2023;415:118085. https://doi.org/10.1016/j.powtec.2022.118085.
[43] Ouadfeul S-A, Aliouane L. Total Organic Carbon Prediction in Shale Gas Reservoirs from Well Logs Data Using the Multilayer Perceptron Neural Network with Levenberg Marquardt Training Algorithm: Application to Barnett Shale. Arab J Sci Eng 2015;40:3345–9. https://doi.org/10.1007/s13369-015-1685-y.
[44] Al HO, Nour AH, Ayodele BV, Bargaa R. Bayesian Regularization-Trained Multi-layer Perceptron Neural Network Predictive Modelling of Phenol Degradation using ZnO/Fe2O3 photocatalyst. J Phys Conf Ser 2020;1529:15–22. https://doi.org/10.1088/1742-6596/1529/5/052058.
[45] Moshkbar-Bakhshayesh K. Bayesian regularization of multilayer perceptron neural network for estimation of mass attenuation coefficient of gamma radiation in comparison with different supervised model-free methods. J Instrum 2020;15:P11019. https://doi.org/10.1088/1748-0221/15/11/P11019.
[46] Yusoff NIM, Ibrahim Alhamali D, Ibrahim ANH, Rosyidi SAP, Abdul HN. Engineering characteristics of nanosilica/polymer-modified bitumen and predicting their rheological properties using multilayer perceptron neural network model. Constr Build Mater 2019;204:781–99. https://doi.org/10.1016/j.conbuildmat.2019.01.203.
[47] Mohd R, Butt MA, Baba MZ. GWLM–NARX: Grey Wolf Levenberg–Marquardt-based neural network for rainfall prediction. Data Technol Appl 2020;54:85–102. https://doi.org/10.1108/DTA-08-2019-0130.
[48] Guzman SM, Paz JO, Tagert MLM. The Use of NARX Neural Networks to Forecast Daily Groundwater Levels. Water Resour Manag 2017;31:1591–603. https://doi.org/10.1007/s11269-017-1598-5.
[49] Jiang J, Wang F, Zhang Y, Qin Y, Gao X. Estimation of Vertical Track Irregularity Based on NARX Neural Network. In: Qin Y, Jia L, Feng J, An M, Diao L, editors. Proc. 2015 Int. Conf. Electr. Inf. Technol. Rail Transp., Berlin, Heidelberg: Springer Berlin Heidelberg; 2016, p. 167–75.
[50] Al Jami A, Himel MU, Hasan K, Basak SR, Mita AF. NARX neural network approach for the monthly prediction of groundwater levels in Sylhet Sadar. Bangladesh J Groundw Sci Eng 2020;8:118–26. https://doi.org/10.19637/j.cnki.2305-7068.2020.02.003.
[51] Nekoee M, Shah-hosseini R. Thermal anomaly detection using NARX neural network method to estimate the earthquake occurrence time. Earth Obs Geomatics Eng 2021;4:98–108. https://doi.org/10.22059/eoge.2021.292253.1067.
[52] Mohammed LB, Hamdan MA, Abdelhafez EA, Shaheen W. Hourly solar radiation prediction based on nonlinear autoregressive exogenous (narx) neural network. Jordan J Mech Ind Eng 2013;7:11–8.
[53] Fan J, Wu L, Zhang F, Cai H, Wang X, Lu X, et al. Evaluating the effect of air pollution on global and diffuse solar radiation prediction using support vector machine modeling based on sunshine duration and air temperature. Renew Sustain Energy Rev 2018;94:732–47.
[54] Ezzeldin R, Hatata A. Application of NARX neural network model for discharge prediction through lateral orifices. Alexandria Eng J 2018;57:2991–8. https://doi.org/10.1016/j.aej.2018.04.001.
[55] Haiqi OA, Nour AH, Ayodele BV, Bargaa R. Bayesian Regularization-Trained Multi-layer Perceptron Neural Network Predictive Modelling of Phenol Degradation using ZnO/Fe 2 O 3 photocatalyst. J Phys Conf Ser 2020;1529(5):052058.
[56] Ayodele BV, Alsaffar MA, Mustapa SI, Kanthasamy R, Wongsakulphasatch S, Cheng CK. Carbon dioxide reforming of methane over Ni-based catalysts: Modeling the effect of process parameters on greenhouse gasses conversion using supervised machine learning algorithms. Chem Eng Process 2021;166:108484. https://doi.org/10.1016/j.cep.2021.108484.
[57] Yang Bo, Li D, Zeng C, Chen Y, Guo Z, Wang J, et al. Parameter extraction of PEMFC via Bayesian regularization neural network based meta-heuristic algorithms. Energy 2021;228:120592.
[58] Aneja S, Sharma A, Gupta R, Yoo D-Y. Bayesian Regularized Artificial Neural Network Model to Predict Strength Characteristics of Fly-Ash and Bottom-Ash Based Geopolymer Concrete. Materials (Basel) 2021;14. doi:10.3390/ma14071729.
[59] Dagdougui H, Bagheri F, Le H, Dessaint L. Neural network model for short-term and very-short-term load forecasting in district buildings. Energy Build 2019;203:109408. https://doi.org/10.1016/j.enbuild.2019.109408.
[60] Taherdangkoo R, Tatomir A, Taherdangkoo M, Qiu P, Sauter M. Nonlinear Autoregressive Neural Networks to Predict Hydraulic Fracturing Fluid Leakage into Shallow Groundwater. Water 2020;12(3):841.